Chemical Engineering Journal 146 (2009) 275–286

Contents lists available at ScienceDirect

Chemical Engineering Journal

journal homepage: www.elsevier.com/locate/cej

Application of periodic operation to kinetic study of NO–CO reaction over Rh/Al_2O_3

Duangkamol Na-Ranong[a,*], Ratanaporn Yuangsawad[a], Prakob Kitchaiya[a], Takashi Aida[b]

[a] Department of Chemical Engineering, Faculty of Engineering, King Mongkut's Institute of Technology Ladkrabang, Chalongkrung Road, Bangkok 10520, Thailand
[b] Department of Chemical Engineering, Tokyo Institute of Technology, O-okayama, Meguro-ku, Tokyo 152-8552, Japan

ARTICLE INFO

Article history:
Received 20 May 2008
Received in revised form 9 September 2008
Accepted 17 September 2008

Keywords:
Reaction mechanism
Parameter determination
NO–CO reaction
Rh/Al_2O_3
Periodic operation

ABSTRACT

A concentration forcing periodic operation has been applied incorporating with a conventional steady-state rate measurement in order to study the kinetics of NO–CO reaction over Rh/Al_2O_3 at 423 K. The steady-state rate data obtained using a differential fixed-bed reactor showed that the order of the reaction was 0 with respect to CO concentration (C_{CO}) and 0.4 with respect to NO concentration (C_{NO}). Under the periodic condition, where a square wave was applied for NO and CO feeding, a deformation of the C_{NO} wave was observed at the outlet of an integral fixed-bed reactor. Shape of the deformed C_{NO} wave indicates that both reactants were strongly adsorbed on catalytic active sites. Three plausible mechanisms that could explain the strong adsorption of these two reactants together with insignificant self-inhibition effect of the strong adsorption on the rate were considered: (I) Langmuir–Hinshelwood (L–H), (II) Eley–Redial-like (E–R-like) and (III) combined L–H and E–R-like mechanisms. A one-dimensional pseudohomogeneous reactor model coupled with the reaction mechanisms was employed to simulate the characteristics of the rate data and the shape of the deformed C_{NO} wave. Only the E–R-like mechanism could predict these characteristics of steady and periodic operations by employing one set of kinetic parameters while the other mechanisms needed different sets of the parameters to predict the characteristics. Sensitivity of each parameter to the shape of the C_{NO} wave was analyzed and value of each parameter was determined for the E–R-like mechanism. The reliabilities of the proposed mechanism and its parameters were evaluated.

1. Introduction

NO–CO reaction over noble metal catalysts (Pt, Pd, Rh, Ru and Ir) has been widely investigated for several decades since it is an important reaction occurring inside automotive catalytic converters [1–7]. Among the noble metal catalysts, Rh is the most appropriated catalyst since it has high stability and activity for reduction of NO with low NH_3 formation. However, incomplete reduction of NO to N_2O at the temperatures below light-off temperature is still the main disadvantage of the catalytic converters. Several efforts have been made to understand the unsteady behaviors of the catalysts since the converters are inevitably operated under unsteady conditions [7–10].

Muraki and Fujitani [10] studied periodic performance of NO–CO reaction over several noble metal catalysts. They found that time-average conversion of NO was remarkably enhanced for Pt whereas it was insignificantly influenced for Rh when NO and CO were alternately introduced into a reactor. This was explained by the degree of alleviation of CO self-poisoning on the catalytic surface by the periodic operation. Our previous work [11] demonstrated that performance of a two-stage catalyst bed reactor operated under a bang–bang periodic condition remarkably depended on the configuration of catalysts placed inside. The reactor having Pt/Al_2O_3 at the inlet-side and Rh/Al_2O_3 at the outlet-side (Pt–Rh) gave time-average conversion of NO higher than the reverse packed one (Rh–Pt). Our work also showed that the C_{NO} wave deformed when NO traveled along with a reactor packed with only Pt or Rh under the periodic condition. The shape of the deformed wave depended on both type and the amount of the catalyst used. In order to clarify these interesting phenomena, a realistic reaction mechanism with appropriate kinetic parameters for each catalyst is necessity.

Information on mechanisms and kinetics of NO–CO reaction over noble metal catalysts were extensively reviewed [3,4,6]. The kinetics of this reaction seems to depend sensitively on types and nature of the employed catalyst (single crystal, polycrystal or supported metal catalyst) and the experimental condition (temperature, pressure and concentration of reactant). Although there are some arguments in the role of each adsorbed species

* Corresponding author. Tel.: +66 2 739 2418; fax: +66 2 739 2418.
E-mail addresses: dnaranong@hotmail.com, knduangk@kmitl.ac.th (D. Na-Ranong).

1385-8947/$ – see front matter © 2008 Elsevier B.V. All rights reserved.
doi:10.1016/j.cej.2008.09.024

Nomenclature

C_i	concentration of component i (mol s^{-1})
$\bar{C}_i$	time-average concentration of component i (mol s^{-1})
F	total volumetric flow rate (m^3 s^{-1})
k_i	rate constant for reaction of ith equation
$k_{a,i}$	rate constant for adsorption of component i (m^3 mol^{-1} s^{-1})
$k_{d,i}$	rate constant for desorption of component i (s^{-1})
n	number of active sites per catalyst weight (mol kg^{-1})
r_{NO}	net rate of reduction of NO (mol kg^{-1} s^{-1})
$r_{c,i}$	net rate of formation of component i (mol kg^{-1} s^{-1})
t	time on stream (s)
W	catalyst weight (kg)
$\bar{X}_{NO}$	time-average conversion of NO (–)

Greek letters

ε	void fraction in catalyst bed, the value of 0.318 was used in the calculation
ρ_P	packing density of catalyst, the value of 550 (kg m^{-3}) was used in the calculation
τ	cycling period (s)
θ_i	surface coverage of component i (–)

Subscript

θ_v	vacant site (–)

among several mechanisms presented in the literature, all the proposed mechanisms were discussed based on reversible adsorption of NO and CO following with Langmuir–Hinshelwood (L–H) or Eley–Redial (E–R) surface reaction steps. Several groups published detailed analysis of the surface reaction steps and reaction mechanism using non-conventional techniques such as transient response method, Monte Carlo simulation, feed composition forcing periodic operation etc. [6,12–18]. Generally, NO dissociation over catalytic site is considered as a key surface reaction step. NO and CO are competitively adsorbed onto the catalytic active sites and their adsorption strength is strong especially under the low temperature region. The two main N-containing products are N_2 and N_2O. The formation of N_2 was considered based on the recombination of N adsorbed atoms (2N-s → N_2 + 2s) or the reaction between molecular adsorbed NO and adsorbed N atom (NO-s + N-s → N_2 + O-s + s). The formation of N_2O was considered based on the reaction between molecular adsorbed NO and adsorbed N atom (NO-s + N-s → N_2O + 2s). The formation of CO_2 is from the reaction between molecular adsorbed CO and O-s which generated from the NO decomposition step (CO-s + O-s → CO_2 + 2s). Unfortunately, we cannot find the reaction model which is well enough to predict the mentioned periodic performance of the two-stage reactor and to simulate the shape of the deformed C_{NO} wave.

We have previously demonstrated that the application of a bang–bang periodic operation was effective to study kinetics of NO–CO reaction over Pt/Al_2O_3 [19]. By analyzing the shape of the deformed C_{NO} wave, we gained useful information on the kinetics and could estimate the kinetic parameters of the proposed mechanism. The result showed that NO–CO reaction over Pt/Al_2O_3 catalyst proceeded via L–H mechanism. Since Rh has similar adsorption characteristics with Pt (NO and CO are competitively adsorbed on active sites and the adsorption strength is strong for both NO and CO), the proposed method was expected to be effective for the case of Rh/Al_2O_3, as well. However, infrared studies showed that several types of adsorbed species which could not be observed on Pt sites were formed on Rh sites during the reaction [15,20–39]. NO is adsorbed on the Pt sites as linear Pt–NO whereas it is adsorbed on the Rh sites as anionic Rh–$NO^{\delta-}$, cationic Rh–$NO^{\delta+}$, neutral Rh–NO and dinytrosyl $Rh(NO)_2$. CO is adsorbed on the Pt sites as linear Pt–CO whereas it is adsorbed on the Rh sites as linear Rh–CO and dicarbonyl $Rh(CO)_2$. The existence of these twin species should make the reaction path of this reaction over Rh/Al_2O_3 more complicated than Pt/Al_2O_3. Consequently, the study of the kinetics of this reaction and the determination of the value of each kinetic parameter based on the application of the bang–bang periodic operation should become more difficult.

The purpose of this work is to demonstrate whether the application of the bang–bang periodic operation is effective for studying the kinetics of NO–CO reaction over Rh/Al_2O_3 or not and to propose a simple reaction mechanism that can predict the steady and periodic behaviors of the reaction. Reaction mechanism and rate parameters are determined by simulating the performance of the reaction under steady and periodic conditions. Sensitivity analysis of parameters is performed in order to verify the model validity.

2. Experimental

The 1 wt% Rh/Al_2O_3 catalyst was prepared by an impregnation method using γ-alumina (JRC-ALO-4, Catalyst Society of Japan, 60–80 mesh) and an aqueous solution of rhodium trichloride ($RhCl_3 \cdot 3H_2O$) as a precursor. The procedure was similar to the one employed for the preparation of 1 wt% Pt/Al_2O_3 in the previous work [19] except that Rh/Al_2O_3 was oxidized in oxygen at 723 K for 3 h and subsequently reduced in hydrogen at 773 K for 3 h. Before each reaction test, the catalyst was pretreated at 723 K in oxygen for 1 h and then hydrogen for 1 h.

A steady-state rate measurement was performed using a differential fixed-bed reactor. The apparatus was the same as the one described in the previous work [40]. The reactor was operated under the isothermal and isobaric condition (423 K, 1 atm). A mixture of reactants (NO/He, CO/He and He as balanced) was introduced into the reactor with a total flow rate of 50 cm^3 min^{-1} (8.33×10^{-7} m^3 s^{-1}) at NTP. The tested range of reactant concentration was 0.022–0.089 mol m^{-3} (500–2000 ppm) for NO and 0.045–0.268 mol m^{-3} (1000–6000 ppm) for CO. Concentration of NO was measured online using a NO_X analyzer (NOA–7000, Shimadzu). Concentration of the other gases in the effluent of the reactor was measured using a gas chromatograph connected with two columns packed with porapak Q and molecular sieve 5A in series. The rate of reaction was calculated from the overall rate of NO reduction ($-r_{NO}$). The selectivity of NO to N_2O (S_{N_2O}) was calculated from $C_{N_2O}/(C_{N_2O} + C_{N_2})$.

A bang–bang periodic operation was conducted by alternately feeding the reactants into an integral reactor packed with 0.5 g of the Rh/Al_2O_3 catalyst. Concentration of each reactant was controlled as a square wave with $\bar{C}_{NO} = 0.041$ mol m^{-3} and $\bar{C}_{CO} = 0.205$ mol m^{-3} by a digital mass flow controller. Nitrogen was employed as a balanced gas and the total flow rate was maintained constant at 50 cm^3 min^{-1} (1.67×10^{-6} m^3 s^{-1}) NTP. The temperature of the catalyst bed was maintained constant at 423 K using a PID controller. The split of NO (S_{NO}) was 0.5 and the phase lag was π radian. The cycling period (τ) varied in the range of 30–180 s. Time-average conversion of NO, $\bar{X}_{NO}$, was calculated from the cycle-invariant C_{NO} wave using Eq. (2-1).

$$\bar{X}_{NO} = \frac{\int_{\tau}^{\tau+1} C_{NO,\,in}\,dt - \int_{\tau}^{\tau+1} C_{NO,\,out}\,dt}{\int_{\tau}^{\tau+1} C_{NO,\,in}\,dt} \quad (2\text{-}1)$$

3. Results and discussion

3.1. Behaviors of the reaction under steady and periodic conditions

Dependence of the steady-state rate of NO reduction ($-r_{NO}$) on the concentration of reactants (C_{CO}, C_{NO}) for Rh catalyst was reported with a simple power rate law ($-r_{NO} = kC_{CO}^{m}\ C_{NO}^{n}$) by several groups. Hendershot and Hanson [41] studied the reaction over Rh(1 0 0) at 688 K and found that the order with respect to C_{CO} (m) varied from +1 to −1 while the order with respect to C_{NO} (n) varied from +1.5 to −1. Hecker and Bell [20] reported insignificant effect of reactant concentration on the steady-state rate over Rh/SiO_2 at 493 K ($m = 0.09$, $n = -0.2$). Granger et al. [42] reported the orders of the reaction over Rh/Al_2O_3 at 573 K; $m = -0.32$ and $n = 0$ to 0.8. Other groups [15,41–43] revealed that the orders sensitively depended on both the nature of employed catalysts and experimental conditions, especially temperature and concentration of reactant. Thus, the $-r_{NO}$ was measured under the ranges of C_{CO} and C_{NO} which covered the concentration change occurring under the periodic condition discussed afterwards.

The steady-state rate measurement was performed under differential conditions. Effects of external and internal mass transfer were neglected in our kinetic analysis since our preliminary experiments showed that the rates insignificantly changed with the feed flow rate and size of the catalyst. Under the steady condition, the conversion of NO sharply decreased with time in the first hour after the reaction started. The conversion further gradually decreased with time on stream and became stationary after 90 min of the reaction time. The rate at this time was calculated and considered as the steady-state rate. The reaction orders with respect to C_{NO} and C_{CO} calculated from the logarithmic plots in Figs. 1 and 2 were 0.396 and −0.002, respectively. The orders were then used as initial estimation for nonlinear regression analysis of a power rate law and we obtained the power rate law expressed as Eq. (3-1) with $R^2 = 0.782$.

$$-r_{NO} = 1.64 \times 10^{-4}\ C_{CO}^{0} C_{NO}^{0.4} \quad (3\text{-}1)$$

The obtained power rate law implied that CO self-poisoning effect on Rh/Al_2O_3 is weaker than the effect on Pt/Al_2O_3 ($m = -0.7$ was reported in Ref. [19]). This difference was discussed as a main reason for the periodic operation effect [10]. In addition, the experimental data showed that S_{N_2O} was in the range of 0.61–1. The high selectivity towards N_2O at low temperatures was also reported by other groups [20,15,46,47].

Under the bang–bang periodic condition with a period of 180 s, the pattern of the C_{NO} wave at the reactor outlet deformed as illustrated in Fig. 3. The time-average conversion of NO ($\bar{X}_{NO}$) was 0.41. In the NO feeding half-cycle, NO was observed in the gas phase after a certain introduction period. This pattern indicates that NO can adsorb onto the catalytic site covered by CO and/or react with the CO that remains on the catalytic sites. In the CO feeding half-cycle, NO suddenly appeared in the gas phase. This was resulted from the flushing of NO by CO. These important characteristics of the response curve implied strong adsorption of the two reactants which agreed well with the information reported in the literature [11,40]. These behaviors are also consistent with the displacement of preadsorbed CO by gaseous NO and the displacement of preadsorbed NO by gaseous CO occurring over Rh/SiO_2 reported by Srinivas et al. [48].Adiabatic raising temperatures (ΔT_{ad}) of overall NO–CO reaction, which consists of two highly exothermic reactions (3-2) and (3-3), was calculated for the extreme cases that $S_{N_2} = 1$ and $S_{N_2O} = 1$.

$$NO + CO \rightarrow 0.5N_2 + CO_2 \quad (\Delta H^{\circ} = -373\ \text{kJ mol}^{-1}) \quad (3\text{-}2)$$

$$NO + 0.5CO \rightarrow 0.5N_2O + 0.5CO_2 \quad (\Delta H^{\circ} = -191\ \text{kJ mol}^{-1}) \quad (3\text{-}3)$$

When the $\bar{X}_{NO}$ was as high as 0.41, at $S_{N_2} = 1$ and $S_{N_2O} = 1$, the ΔT_{ad} were 5.1 and 2.6 K, respectively. Experimentally, it should be

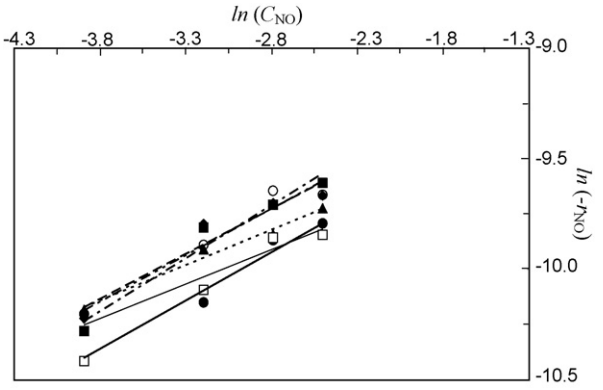

Fig. 2. Logarithmic plot of the reaction rate and NO concentration for various C_{CO} (mol m^{-3}): 0.0409; (●, —); 0.0613 (♦, – – –); 0.1022 (▲, - - -); 0.1431 (■, –·–·–); 0.2045 (○, –···–); 0.2454 (□, —).

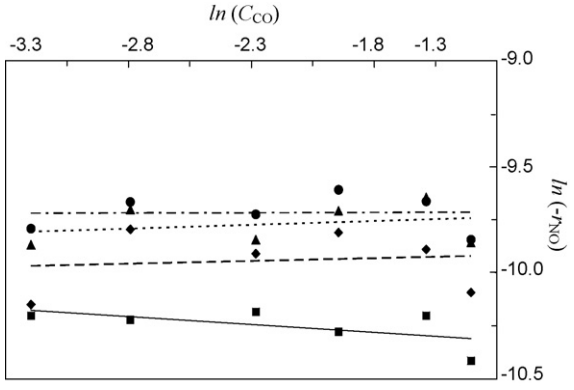

Fig. 1. Logarithmic plot of the reaction rate and CO concentration for various C_{NO} (mol m^{-3}): 0.0204 (■, —); 0.0409 (♦, – – –); 0.0613 (▲, - - -); 0.0818 (●, –·–·).

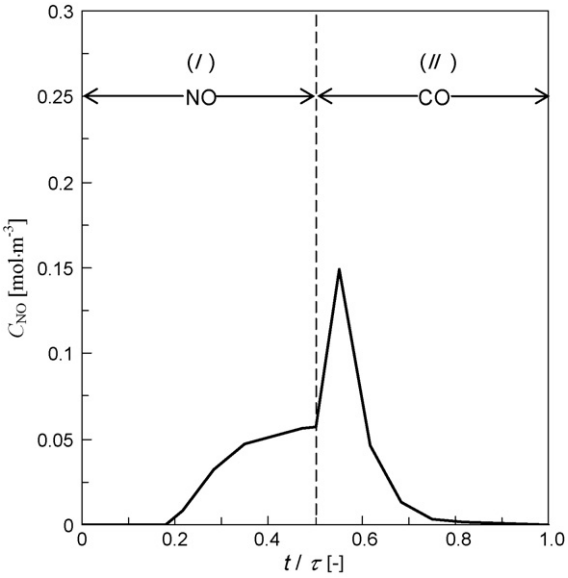

Fig. 3. NO concentration experimentally observed as a function of time on stream at outlet of the reactor.

noted that in the tested range, S_{N_2O} varied from 0.61 to 1 under non-adiabatic condition.

In general, a rate of reaction is suppressed by adsorption of the reactant strongly adsorbed on catalytic sites. However, our experimental results showed that both NO and CO were strongly adsorbed onto the Rh sites but the rate was insignificantly suppressed by adsorption of neither NO nor CO. As mentioned in Section 1 that each active site on Rh/Al_2O_3 under these conditions can simultaneously adsorb two molecules of NO as Rh–$(NO)_2$ for NO adsorption or two molecules of CO as Rh–$(CO)_2$ for CO adsorption. Although we did not observe the band corresponding to NO–Rh–CO in IR spectrum [25], NO–Rh–CO may be formed during the reaction because the molecules of NO and CO are similar. There are other reports of the formation of this species on catalytic sites of Rh/Al_2O_3 appeared in the literature [21,49–51]. NO–Rh–CO was considered as an intermediate of the reaction. Therefore, we believe that NO–Rh–CO is formed and the absence of its IR band should be due to the rapid consumption of this species during the reaction. In addition, the formation of NO–Rh–CO should be the reason of insignificant suppression of the rate by either NO or CO despite the strong adsorption of the two reactants onto catalytic sites.

3.2. Mechanism of the surface reaction

Elementary surface reactions considered in the literature [3–6] could be summarized as follows:

$$NO + s \rightleftharpoons NO\text{-}s \quad (1)$$

$$CO + s \rightleftharpoons CO\text{-}s \quad (2)$$

$$CO\text{-}s + NO\text{-}s \rightarrow CO_2 + N\text{-}s + s \quad (3)$$

$$CO + NO\text{-}s \rightarrow CO_2 + N\text{-}s \quad (4)$$

$$CO\text{-}s + NO \rightarrow CO_2 + N\text{-}s \quad (5)$$

$$2NO\text{-}s \rightarrow N_2 + 2O\text{-}s \quad (6)$$

$$2NO\text{-}s \rightarrow N_2O + O\text{-}s + s \quad (7)$$

$$NO\text{-}s + s \rightarrow N\text{-}s + O\text{-}s \quad (8)$$

$$NO\text{-}s + N\text{-}s \rightarrow N_2O + 2s \quad (9)$$

$$NO\text{-}s + N\text{-}s \rightarrow N_2 + O\text{-}s + s \quad (10)$$

$$2N\text{-}s \rightarrow N_2 + 2s \quad (11)$$

$$CO\text{-}s + O\text{-}s \rightarrow CO_2 + 2s \quad (12)$$

$$CO\text{-}s + N\text{-}s \rightarrow NCO\text{-}s + s \quad (13)$$

It is general agreement that both NO and CO are reversibly adsorbed on active sites (Steps (1) and (2)). Several groups showed that the rate of NO dissociation was very slow and considered this step as a rate-determining step in the NO–CO reaction over Rh catalysts [3]. TPD spectra reported by Dubois et al. [52] showed that the dissociation of NO started at 450 K. The NO dissociation may be blocked due to the presence of neighboring co-adsorbed NO and CO [53–56]. Belton's group showed that adsorbed NO strongly inhibited the NO dissociation over Pt–Rh alloy catalyst. Since our experiments were conducted at the temperature below 450 K, the catalytic surface should be almost completely covered by adsorbed species and hence the neighboring vacant sites which can participate in the NO dissociation should be hardly found. For these reasons, Step (8) was omitted from our discussion. Infrared spectroscopic studies have reported the formation of isocyanate (NCO) on Rh surface and its migration to the support [22,23,57–61]. The intensity of their corresponding IR bands increased with increasing reaction temperature. However, the role of these species on the NO–CO reaction is still unclear whether it is an active intermediate or not. Our preliminary IR observation [25] showed very small peaks of isocyanate species at 2233 and 2254 cm^{-1} during the reaction at 423 K. Therefore, the steps involving formation and consumption of isocyanate species were not considered in our discussion. Chuang and coworkers discussed activity of $Rh(CO)_2$ based on a redox mechanism [22,62]. They explained that $Rh(CO)_2$ rapidly reacted with oxygen (O-s) generated from NO dissociation and $Rh(CO)_2$ was not active at the condition under which the NO dissociation did not occur. Since the NO dissociation was omitted from our discussion, no O-s was formed on the catalytic surface. Our previous work [25] also showed that $Rh(CO)_2$ was formed during the reaction but the intensity of its IR band was not influenced by the change in the feed composition. On the other hand, the changing in the intensity of Rh–CO band corresponded well with the response of the CO_2 concentration in the gaseous product. Therefore, it is reasonable to assume that $Rh(CO)_2$ is not an intermediate and hence the steps involving its formation and consumption should not play any roles on the surface catalytic cycle to produce CO_2, N_2 and N_2O. However, the accumulation of $Rh(CO)_2$ should be considered as a reason of the decrease of rate with time on stream mentioned in Section 3.1.

Several combinations of the elementary steps (Steps (1)–(13)) were considered. Only three plausible mechanisms could explain the important characteristics of the steady and periodic behaviors described in Section 3.1 and were selected for further discussion.

Mechanism I

$$NO + s \underset{k_{d,NO}}{\overset{k_{a,NO}}{\rightleftharpoons}} NO\text{-}s \quad (1)$$

$$CO + s \underset{k_{d,CO}}{\overset{k_{a,CO}}{\rightleftharpoons}} CO\text{-}s \quad (2)$$

$$CO\text{-}s + NO\text{-}s \xrightarrow{k_3} CO_2 + N\text{-}s + s \quad (3)$$

$$NO\text{-}s + N\text{-}s \xrightarrow{k_9} N_2O + 2\,s \quad (9)$$

$$2N\text{-}s \xrightarrow{k_{11}} N_2 + 2\,s \quad (11)$$

Mechanism II

$$NO + s \underset{k_{d,NO}}{\overset{k_{a,NO}}{\rightleftharpoons}} NO\text{-}s \quad (1)$$

$$CO + s \underset{k_{d,CO}}{\overset{k_{a,CO}}{\rightleftharpoons}} CO\text{-}s \quad (2)$$

$$CO + NO\text{-}s \xrightarrow{k_4} CO_2 + N\text{-}s \quad (4)$$

$$CO\text{-}s + NO \xrightarrow{k_5} CO_2 + N\text{-}s \quad (5)$$

$$NO\text{-}s + N\text{-}s \xrightarrow{k_9} N_2O + 2\,s \quad (9)$$

$$2N\text{-}s \xrightarrow{k_{11}} N_2 + 2\,s \quad (11)$$

Mechanism III

$$NO + s \underset{k_{d,NO}}{\overset{k_{a,NO}}{\rightleftharpoons}} NO\text{-}s \quad (1)$$

$$CO + s \underset{k_{d,CO}}{\overset{k_{a,CO}}{\rightleftharpoons}} CO\text{-}s \quad (2)$$

$$CO\text{-}s + NO\text{-}s \xrightarrow{k_3} CO_2 + N\text{-}s + s \quad (3)$$

$$CO + NO\text{-}s \xrightarrow{k_4} CO_2 + N\text{-}s \quad (4)$$

$$\text{CO-s} + \text{NO} \xrightarrow{k_5} \text{CO}_2 + \text{N-s} \quad (5)$$

$$\text{NO-s} + \text{N-s} \xrightarrow{k_9} \text{N}_2\text{O} + \text{s} \quad (9)$$

$$2\text{N-s} \xrightarrow{k_{11}} \text{N}_2 + 2\,\text{s} \quad (11)$$

Steps (1) and (2) represent reversible adsorption of NO and CO, respectively. In every mechanism, we assume that there is only one type of active sites which NO and CO is competitively adsorbed and their adsorptions occur without self-dissociation. To simplify the reaction mechanism only NO-s, CO-s and N-s are considered as adsorbed species. N_2O, N_2 and CO_2 are the products. N_2O is produced from NO-s and N-s (Step (9)). N_2 is produced by the recombination of N-s as in Step (11).

These three mechanisms mainly differ on two points: (i) the amount of active sites required for the reaction and (ii) the way that the two reactants react together. For Mechanism I, each reactant is firstly adsorbed onto an active site and the adsorbed molecules successively react together via Step (3). Two active sites are required for the reaction. This is known as Langmuir–Hinshelwood (L–H) mechanism. For Mechanism II, only one active site is required for the reaction between NO and CO. As discussed in Section 3.1 that NO–Rh–CO is formed and rapidly consumed during the reaction, we assume that NO–Rh–CO is formed via Step (18) and consumed via Step (19).

$$\begin{array}{l} \text{CO} + \text{NO-s} \xrightarrow{\text{slow}} \\ \qquad\qquad \text{NO-s-CO} \\ \text{CO-s} + \text{NO} \xrightarrow{\text{slow}} \end{array} \quad (18)$$

$$\text{NO-s-CO} \xrightarrow{\text{fast}} \text{CO}_2 + \text{N-s} \quad (19)$$

The addition of these two steps into the reaction mechanism results in two different types of active site which gaseous NO or CO can be adsorbed. One is a vacant site and the other is a preadsorbed site. The existence of the two types of active site makes solving steady-state rate expression of Mechanisms II and III much more difficult. Fortunately, we can simplify these two successive steps as Step (4) or Step (5) because the rate of Step (18) is much slower than Step (19). The simplification represented by Steps (4) and (5) are Eley–Redial-like (E–R-like) steps. We assume that Steps (4) and (5) proceed with the same rate. For Mechanism III, Steps (3)–(5) are considered. In other words, the rates of L–H step and E–R-like step are comparable and the reactants are consumed by both L–H and E–R-like mechanisms.

The steady-state rate expression for each reaction mechanism was derived based on equilibrium adsorptions of NO and CO. The obtained rate expression for each mechanism is summarized in Table 1.

3.3. Model discrimination and parameter determination

In order to discriminate the reaction mechanisms, the steady-state rate and the shape of the C_{NO} wave in Fig. 3 were calculated according to each mechanism. The C_{NO} wave at the outlet of the reactor operated under the periodic condition was calculated using a one-dimensional pseudohomogeneous model of an integral plug-flow reactor operated under an isothermal condition. The mass conservation of species "i" in gas phase is expressed as Eq. (20). The balances of the surface species for each mechanism are expressed in Eqs. (3-4)–(3-14).

$$\frac{\partial C_i}{\partial t} = -\frac{\rho_P}{\varepsilon}\left(F\frac{\partial C_i}{\partial W} + r_{c,i}\right) \quad (3\text{-}4)$$

where

$$r_{c,i} = n(k_{a,i}C_i\theta_v - k_{d,i}\theta_i) \quad (3\text{-}5)$$

Mechanism I

$$\frac{d\theta_{NO}}{dt} = k_{a,NO}C_{NO}\theta_v - k_{d,NO}\theta_{NO} - k_3\theta_{CO}\theta_{NO} - k_9\theta_{NO}\theta_N \quad (3\text{-}6)$$

$$\frac{d\theta_{CO}}{dt} = k_{a,CO}C_{CO}\theta_v - k_{d,CO}\theta_{CO} - k_3\theta_{CO}\theta_{NO} \quad (3\text{-}7)$$

$$\frac{d\theta_N}{dt} = k_3\theta_{NO}\theta_{CO} - k_9\theta_{NO}\theta_N - k_{11}\frac{\theta_N^2}{2} \quad (3\text{-}8)$$

Mechanism II

$$\frac{d\theta_{NO}}{dt} = k_{a,NO}C_{NO}\theta_v - k_{d,NO}\theta_{NO} - k_4C_{CO}\theta_{NO} - k_9\theta_{NO}\theta_N \quad (3\text{-}9)$$

$$\frac{d\theta_{CO}}{dt} = k_{a,CO}C_{CO}\theta_v - k_{d,CO}\theta_{CO} - k_5C_{NO}\theta_{CO} \quad (3\text{-}10)$$

$$\frac{d\theta_N}{dt} = k_4C_{CO}\theta_{NO} + k_5C_{NO}\theta_{CO} - k_9\theta_{NO}\theta_N - k_{11}\frac{\theta_N^2}{2} \quad (3\text{-}11)$$

Mechanism III

$$\frac{d\theta_{NO}}{dt} = k_{a,NO}C_{NO}\theta_v - k_{d,NO}\theta_{NO} - k_3\theta_{CO}\theta_{NO} - k_4C_{CO}\theta_{NO} - k_9\theta_{NO}\theta_N \quad (3\text{-}12)$$

$$\frac{d\theta_{CO}}{dt} = k_{a,CO}C_{CO}\theta_v - k_{d,CO}\theta_{CO} - k_3\theta_{CO}C_{NO} - k_5C_{NO}\theta_{CO} \quad (3\text{-}13)$$

$$\frac{d\theta_N}{dt} = k_3\theta_{NO}\theta_{CO} + k_4C_{CO}\theta_{NO} + k_5C_{NO}\theta_{CO} - k_9\theta_{NO}\theta_N - k_{11}\frac{\theta_N^2}{2} \quad (3\text{-}14)$$

These equations were simultaneously solved with FORTRAN90 programming using a finite difference method.

The steady-state rate was calculated using the rate expression listed in Table 1. By varying the value of parameters, we

Table 1
Rate expressions of the NO–CO reaction over Rh/Al_2O_3 corresponding to Mechanisms I, II and III.

Variable	Model		
	[I] $-r_{NO} = n(k_3\theta_{NO}\theta_{CO} + k_9\theta_{NO}\theta_N)$	[II] $-r_{NO} = 2n(k_{11}\theta_N^2 + k_9\theta_{NO}\theta_N)$	[III] $-r_{NO} = 2n(k_{11}\theta_N^2 + k_9\theta_{NO}\theta_N)$
θ_{NO}	$K_{NO}C_{CO}\theta_v$	$K_{NO}C_{CO}\theta_v$	$K_{NO}C_{CO}\theta_v$
θ_{CO}	$K_{CO}C_{CO}\theta_v$	$K_{CO}C_{CO}\theta_v$	$K_{CO}C_{CO}\theta_v$
θ_N	$\theta_v\alpha$	$1-(K_{NO}C_{NO}+K_{CO}C_{CO}+1)\theta_v$	$1-(K_{NO}C_{NO}+K_{CO}C_{CO}+1)\theta_v$
θ_v	$\frac{1}{(A+\alpha)^2}$	$\frac{-b-\sqrt{b^2-4ac}}{2a}$	$\frac{-b-\sqrt{b^2-4ac}}{2a}$
a	–	$A^2k_{11} - 2Ak_9K_{NO}C_{NO}$	$A^2k_{11} - 2Ak_9K_{NO}C_{NO} - 2k_3K_{NO}K_{CO}C_{NO}C_{CO}$
b	–	$2k_9K_{NO}C_{NO} - 2Ak_{11} - 2k_4K_{CO}C_{CO}C_{NO} - 2k_5K_{NO}C_{NO}C_{CO}$	$2k_9K_{NO}C_{NO} - 2Ak_{11} - 2k_4K_{CO}C_{CO}C_{NO} - 2k_5K_{NO}C_{NO}C_{CO}$
c	–	k_2	k_2
A	$1 + K_{NO}C_{NO} + K_{CO}C_{CO}$	$1 + K_{NO}C_{NO} + K_{CO}C_{CO}$	$1 + K_{NO}C_{NO} + K_{CO}C_{CO}$

$\alpha = \frac{\sqrt{(k_9K_{NO}C_{NO})^2 + 4k_3k_{11}K_{NO}K_{CO}C_{NO}C_{CO}} - k_9K_{NO}C_{NO}}{2k_{11}}$.

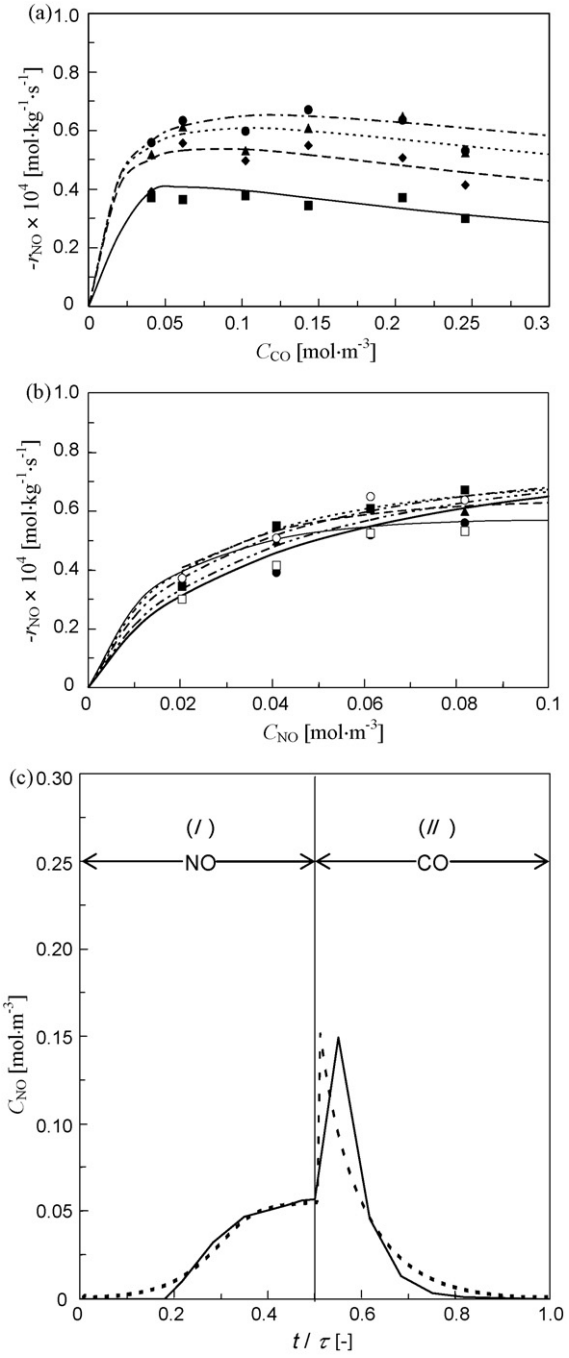

Fig. 4. Comparison of the results calculated based on Mechanism I with the experimental ones. The parameters listed in Tables 2 and 3 were used for the calculation of the steady-state rate and the NO concentration wave, respectively. (a) Dependence of reaction rate on concentration of CO for various C_{NO} at steady state: C_{NO} (mol m^{-3}): 0.0205 (■, —); 0.0409 (♦, – – –); 0.0613 (▲, - - -); 0.0818 (●, –·–·), (b) dependence of reaction rate on concentration of NO for various C_{CO} at steady state: C_{CO} (mol m^{-3}): 0.0409 (●, —); 0.0613 (♦, – – –); 0.1022; (▲, - - -); 0.1431 (■, –·–·); 0.2045 (○, –··–); 0.2454 (□, —), and (c) NO concentration wave observed at the reactor outlet under bang–bang periodic condition: (—) experimental results; (- - -) calculated results.

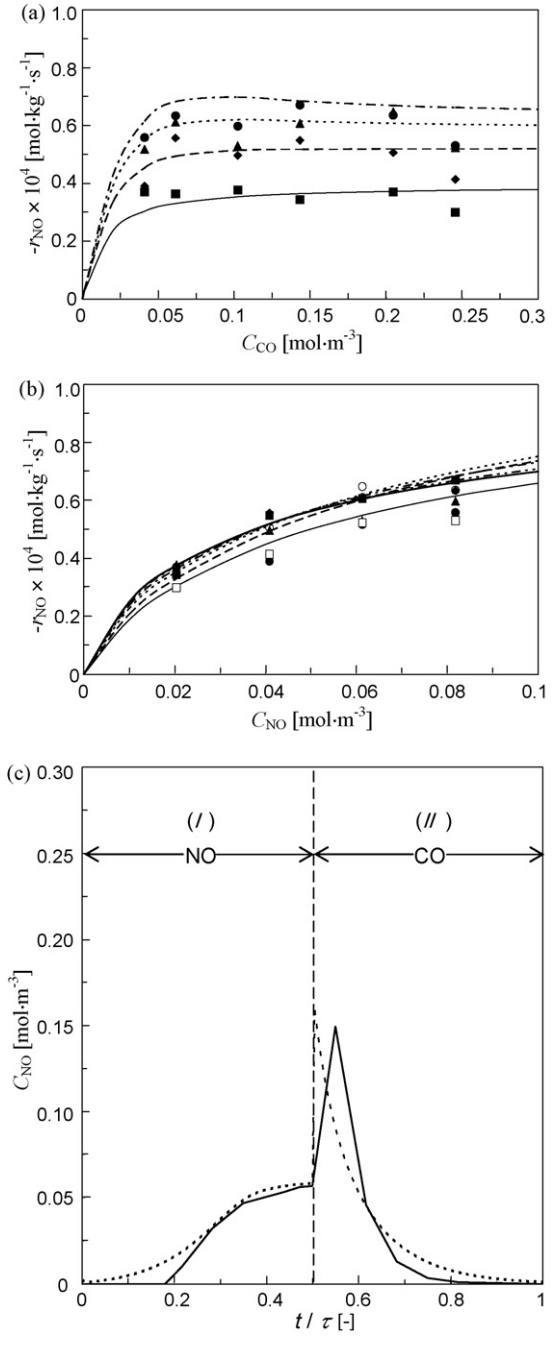

Fig. 5. Comparison of the results calculated based on Mechanism II with the experimental ones. The parameters listed in Tables 2 and 3 were used for the calculation of the steady-state rate and the NO concentration wave, respectively. (a) Dependence of reaction rate on concentration of CO for various C_{NO} at steady state: C_{NO} (mol m^{-3}): 0.0205 (■, —); 0.0409 (♦, – – –); 0.0613 (▲, - - -); 0.0818 (●, –·–), (b) dependence of reaction rate on concentration of NO for various C_{CO} at steady state: C_{CO} (mol m^{-3}): 0.0409 (●, —); 0.0613 (▲, - - -); 0.1431 (■, –·–); 0.2045 (○, –··–); 0.2454 (□, —), and (c) NO concentration wave observed at the reactor outlet under bang–bang periodic condition: (—) experimental results; (- - -) calculated results.

found the set of parameters that can reproduce the dependence of the $-r_{NO}$ on C_{NO} and C_{CO} for all of the assumed mechanisms, as illustrated in Figs. 4–6 Figs. 4(a)-(b), 5(a)-(b) and 6(a)-(b). The parameters providing the best fit of the steady-state data for each mechanism are summarized in Table 2. The simulated curves in Figs. 4(a), 5(a) and 6(a) show that the $-r_{NO}$ is almost constant with respect to C_{CO} when C_{CO} is higher than 0.05 mol m^{-3}. The simulated curves in Figs. 4(b), 5(b) and 6(b) show that the rate gradually increases with increasing the C_{NO} in all tested range for every assumed mechanism.

The calculated results of C_{NO} wave are shown in Figs. 4(c), 5(c) and 6(c) for Mechanisms I, II and III, respectively. All of the assumed mechanisms can provide the shape of the

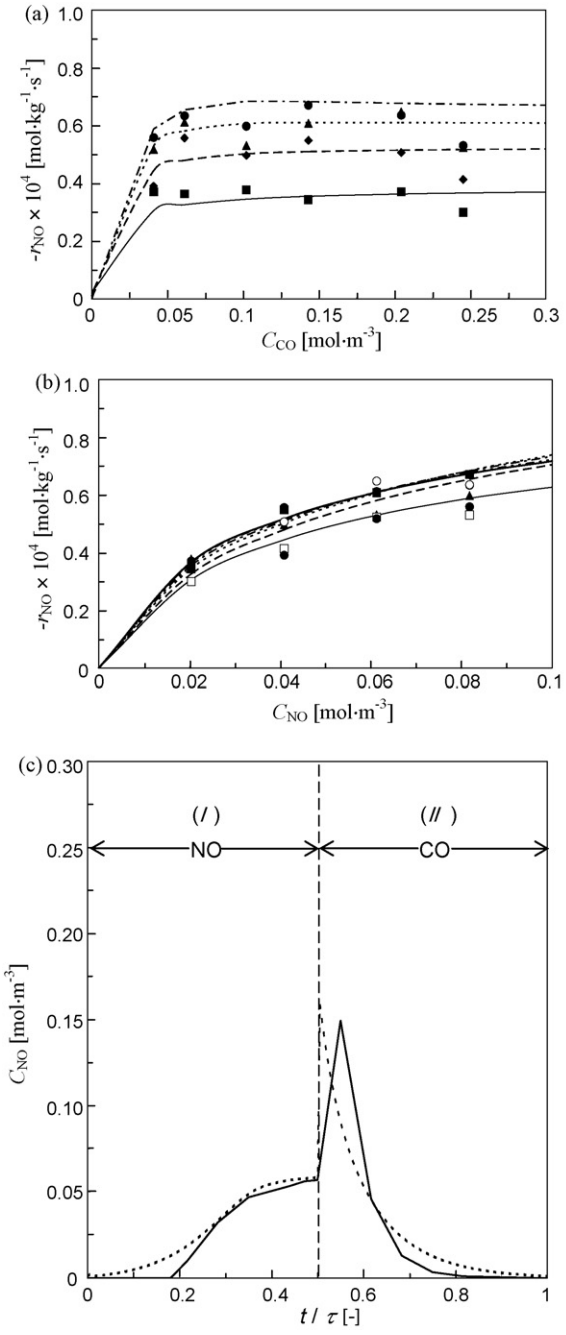

Fig. 6. Comparison of the results calculated based on Mechanism III with the experimental ones. The parameters listed in Tables 2 and 3 were used for the calculation of the steady-state rate and the NO concentration wave, respectively. (a) Dependence of reaction rate on concentration of CO for various C_{NO} at steady state: C_{NO} (mol m^{-3}): 0.0205 (■, —); 0.0409 (♦, – – –); 0.0613 (▲, - - -); 0.0818 (●, –·–·), (b) dependence of reaction rate on concentration of NO for various C_{CO} at steady state: C_{CO} (mol m^{-3}): 0.0409 (●, —); 0.0613 (♦, – – –); 0.1022 (▲, - - -); 0.1431 (■, –·–); 0.2045 (○, –··–); 0.2454 (□, —), and (c) NO concentration wave observed at the reactor outlet under bang–bang periodic condition: (—) experimental results; (- - -) calculated results.

deformed C_{NO} wave that matches with the experimental result. The parameters providing the best fit of the C_{NO} wave for each mechanism are summarized in Table 3. The C_{NO} wave in the NO feeding half-cycle ($0 \le t/\tau \le 0.5$) is like *S*-shape. When the feeding was switched from NO to CO, NO suddenly appeared in the gas phase. After C_{NO} reached the maximum value, which exceeded the value in the feed, C_{NO} gradually decreased. These are important

Table 2
Parameters providing the best fit of steady-state rate data according to each mechanism.

Parameter	Mechanism I	Mechanism II	Mechanism III
K_{NO}	25	100	100
K_{CO}	20	110	110
k_3	0.05	–	0.001
k_4, k_5	–	0.04	0.035
k_9	0.0035	0.01	0.0095
k_{11}	0.0015	0.002	0.0022
n	0.0205	0.0205	0.0205

Table 3
Parameters providing the best fit of the shape of C_{NO} wave under periodic condition according to each mechanism.

Parameter	Mechanism I	Mechanism II	Mechanism III
$k_{a,NO}$	38	38	38
$k_{d,NO}$	0.05	0.05	0.05
$k_{a,CO}$	95	95	95
$k_{d,CO}$	0.34	0.34	0.34
k_3	0.05	–	0.000001
k_4, k_5	–	0.035	0.035
k_9	0.0095	0.009	0.009
k_{11}	0.0018	0.0004	0.0004
n	0.0205	0.0205	0.0205

characteristics of the experimentally observed shape of the C_{NO} wave that can be reproduced reasonably well by the simulations. However, at the time that the NO feed was switched to the CO one, the simulation result show the immediate increase in C_{NO} (slope = ∞) which does not match with the experimental result. This discrepancy between the slopes should be caused by axial dispersion occurring in the real fixed-bed reactor while we used an ideal plug-flow reactor model.

Although we found that all the assumed mechanisms can reproduce characteristics of the steady and periodic behaviors of the reaction, the value of the parameters should not depend on the mode of operation. Therefore, the calculation was further performed and the parameters were adjusted in order to find the set of the parameters which can provide good resemblance of the experimental and the calculated results under both steady and periodic conditions. For Mechanism I, we cannot find any set of the parameters that gave good resemblance for both conditions. The best fit of the results obtained from the calculation with one set of the parameters (in Table 4) for Mechanism I is illustrated in Fig. 7. It reveals that the calculation shows good resemblance only for periodic behavior whereas the calculated rate data remarkably deviates from the experimental ones. This indicates that Mechanism I is incorrect so it is discarded from the discussion in this study. On the contrary, both steady and periodic behaviors were satisfactorily reproduced with the same set of the parameters when the calcu-

Table 4
Parameters providing the best fit of both steady state and periodic C_{NO} wave according to each mechanism.

Parameter	Mechanism I	Mechanism II	Mechanism III
$k_{a,NO}$	38	38	38
$k_{d,NO}$	0.0475	0.05	0.05
K_{NO}	800	760	760
$k_{a,CO}$	95	95	95
$k_{d,CO}$	0.32	0.34	0.34
K_{CO}	297	279	279
k_3	0.055	–	0.000001
k_4, k_5	–	0.030	0.03
k_9	0.0085	0.010	0.01
k_{11}	0.002	0.0006	0.0006
n	0.0205	0.0205	0.0205

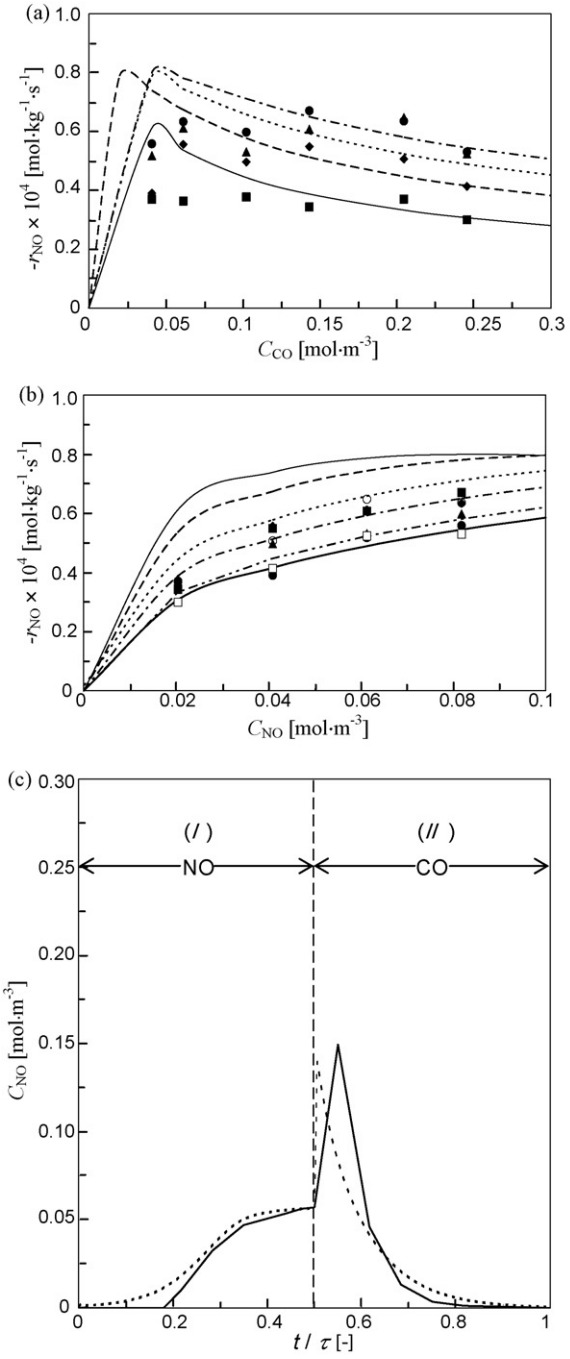

Fig. 7. Comparison of the results calculated based on Mechanism I with the experimental ones. The parameters listed in Table 4 were used for the calculations. (a) Dependence of reaction rate on concentration of CO for various C_{NO} at steady state: C_{NO} (mol m^{-3}): 0.0205 (■, —); 0.0409 (♦, – – –); 0.0613 (▲, - - -); 0.0818 (●, –·–), (b) dependence of reaction rate on concentration of NO for various C_{CO} at steady state: C_{CO} (mol m^{-3}): 0.0409 (●, —); 0.0613 (♦, – – –); 0.1022 (▲, - - -); 0.1431 (■, –·–); 0.2045 (○, –··–); 0.2454 (□, —), and (c) NO concentration wave observed at the reactor outlet under bang–bang periodic condition: (—) experimental results; (- - -) calculated results.

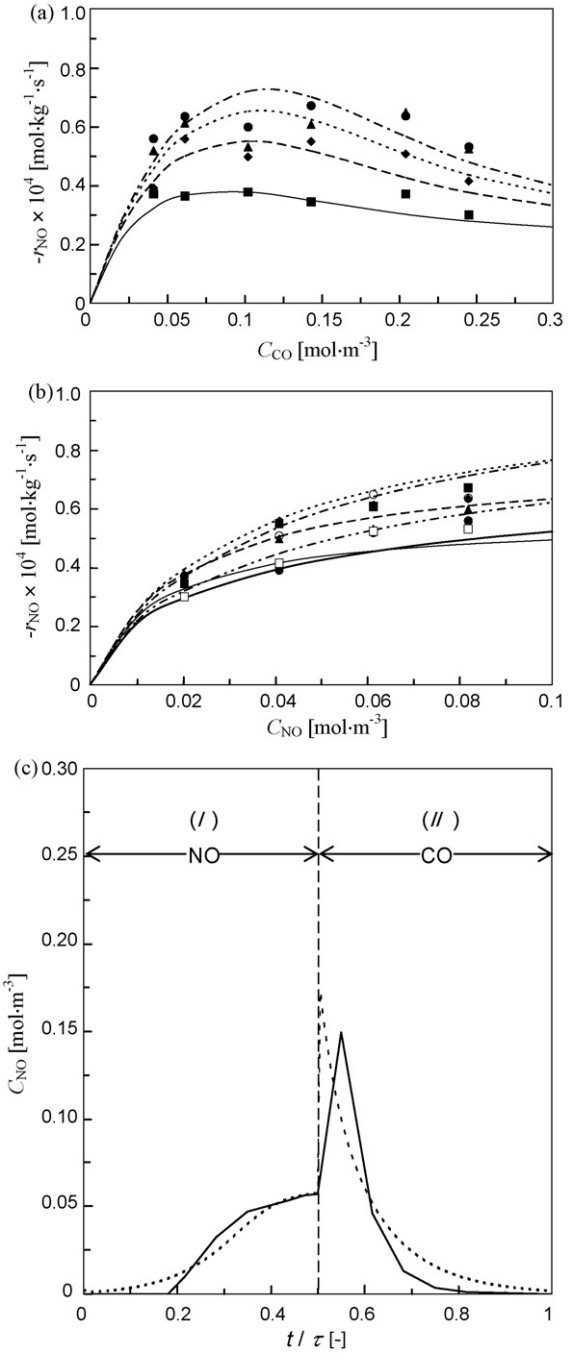

Fig. 8. Comparison of the results calculated based on Mechanism II with the experimental ones. The parameters listed in Table 4 were used for the calculations. (a) Dependence of reaction rate on concentration of CO for various C_{NO} at steady state: C_{NO} (mol m^{-3}): 0.0205 (■, —); 0.0409 (♦, – – –); 0.0613 (▲, - - -); 0.0818 (●, –·–·), (b) dependence of reaction rate on concentration of NO for various C_{CO} at steady state: C_{CO} (mol m^{-3}): 0.0409 (●, —); 0.0613 (♦, – – –); 0.1022 (▲, - - -); 0.1431 (■, –·–·); 0.2045 (○, –··–); 0.2454 (□, —), and (c) NO concentration wave observed at the reactor outlet under bang–bang periodic condition: (—) experimental results; (- - -) calculated results.

lations were performed according to Mechanism II. Fig. 8 shows the calculated results comparing with the experimental ones. The set of parameters that provides the best fit of the results is listed in Table 4. The deviation of the C_{NO} wave is 0.0026. The calculated curves in Fig. 8(a) show that $-r_{NO}$ slightly depends on C_{NO}. The highest point of the $-r_{NO}$ curve slightly shifts to the right when the C_{NO} increases. The calculated curves in Fig. 8(b) show that $-r_{NO}$ gradually increases with increasing C_{NO}. All characteristics of the shape of the deformed C_{NO} wave can be reproduced reasonably well by the simulation. Accordingly, Mechanism II should be left for further analysis. Sensitivity analysis for this mechanism will be performed and discussed in Section 3.4. As for Mechanism III, the simulation could reproduce the experimental results only when k_3 was much less than k_4. This result indicates that the reaction between NO and

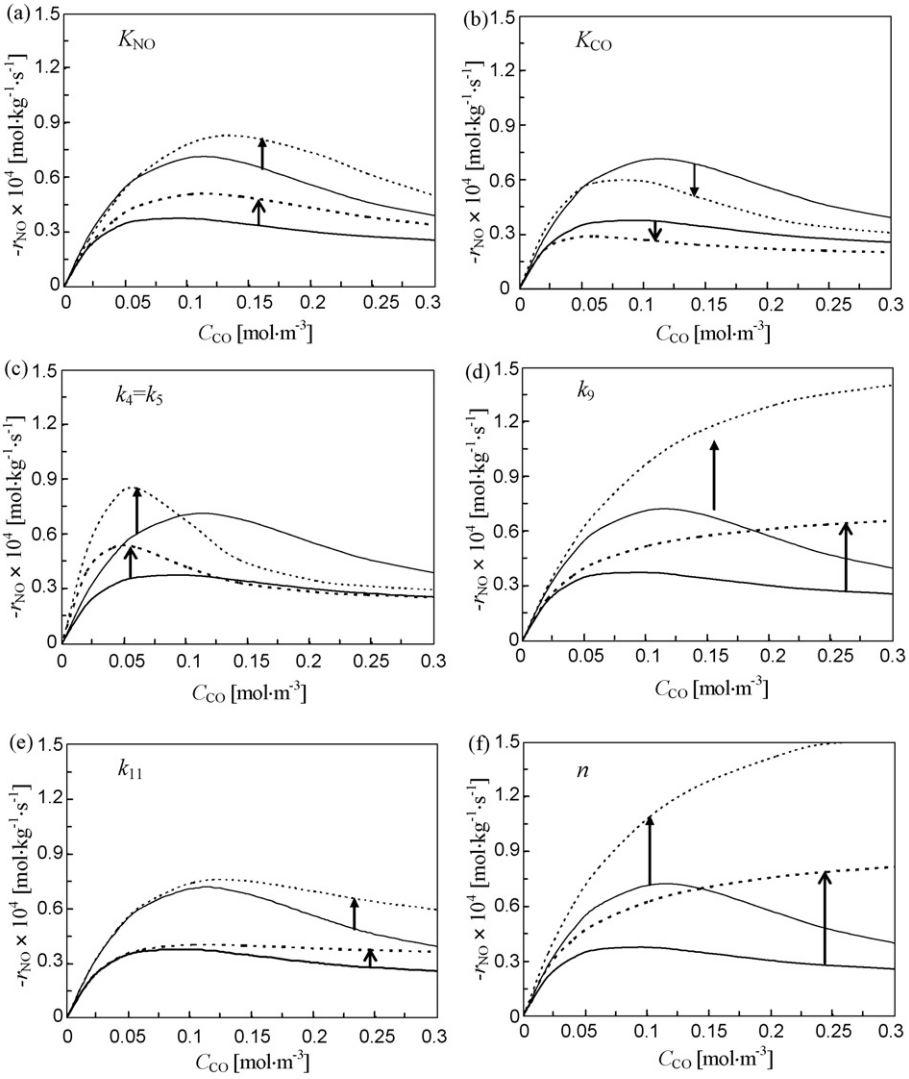

Fig. 9. Sensitivity of each parameter in Mechanism II to the shape of the curves representing dependence of steady-state rate on C_{CO} for various C_{NO}: 0.0205 (—, ···); 0.0818 (**—**, ···). Lines were given for the calculation using the parameters listed in Table 4. Dotted lines were for double value of the parameters listed in Table 4.

CO occurs mainly via Step (4) or Step (5). In other words, Mechanism III could be used to predict the reaction behavior only when it is exactly the same as Mechanism II. Therefore, Mechanism III is also discarded from our discussion.

3.4. Sensitivity analysis for the proposed model

In this section, the sensitivity of each parameter to the shape of the calculated curves representing the steady and periodic behaviors is analyzed for Mechanism II.

Fig. 9 shows that each parameter affects the shape of the calculated curves of steady-state rate in a different way. The increase of K_{NO} results in increasing the reaction rate and shifting the maximum rate to the right while the increase of K_{CO} results in decreasing the reaction rate and shifting the maximum rate to the left. The increase of k_4 causes the maximum rate to increase and shift to the left. The increases of k_9 and n result in increasing the reaction rate throughout the observed range of C_{CO}. k_{11} insignificantly affects the maximum rate. Increasing of k_{11} gradually increases the reaction rate as C_{CO} is increased.

Fig. 10 shows that each parameter affects the shape of the calculated C_{NO} wave differently. $k_{a,NO}$, $k_{a,CO}$, $k_{d,CO}$ and k_9 mainly affect the shape of the C_{NO} wave in Region I. The higher value the $k_{a,NO}$ or $k_{d,CO}$ is, the longer the introduction period and the steeper the slope of C_{NO} are. Increasing the value of $k_{a,CO}$ results in changing the shape of the C_{NO} wave. Increasing the value of k_9 decreases C_{NO}. The $k_{d,NO}$ mainly affects the shape of the C_{NO} wave in Region II. The larger the $k_{d,NO}$ is, the higher spike of the C_{NO} wave is. k_4, k_5 and n affect the shape of C_{NO} wave in both Regions I and II. The greater values of k_4 and k_5 result in the increase of C_{NO} detected in Region I and the rapid decrease of C_{NO} detected in Region II. When n is increased, C_{NO} in Region I decreases and the decreasing rate of C_{NO} in Region II becomes slower. k_{11} is only one rate parameter in this model that does not affect the shape of C_{NO} wave.

The results in Figs. 9 and 10 reveal that most of the parameters in Mechanism II sensitively affect the shape of the calculated curves representing both steady and periodic behaviors of this reaction. Therefore, the parameters obtained from analyzing both steady and periodic data should be appropriate.

3.5. Evaluation of model reliability

The set of parameters for Mechanism II listed in Table 4 should give useful kinetic information of the reaction. The obtained K_{NO}

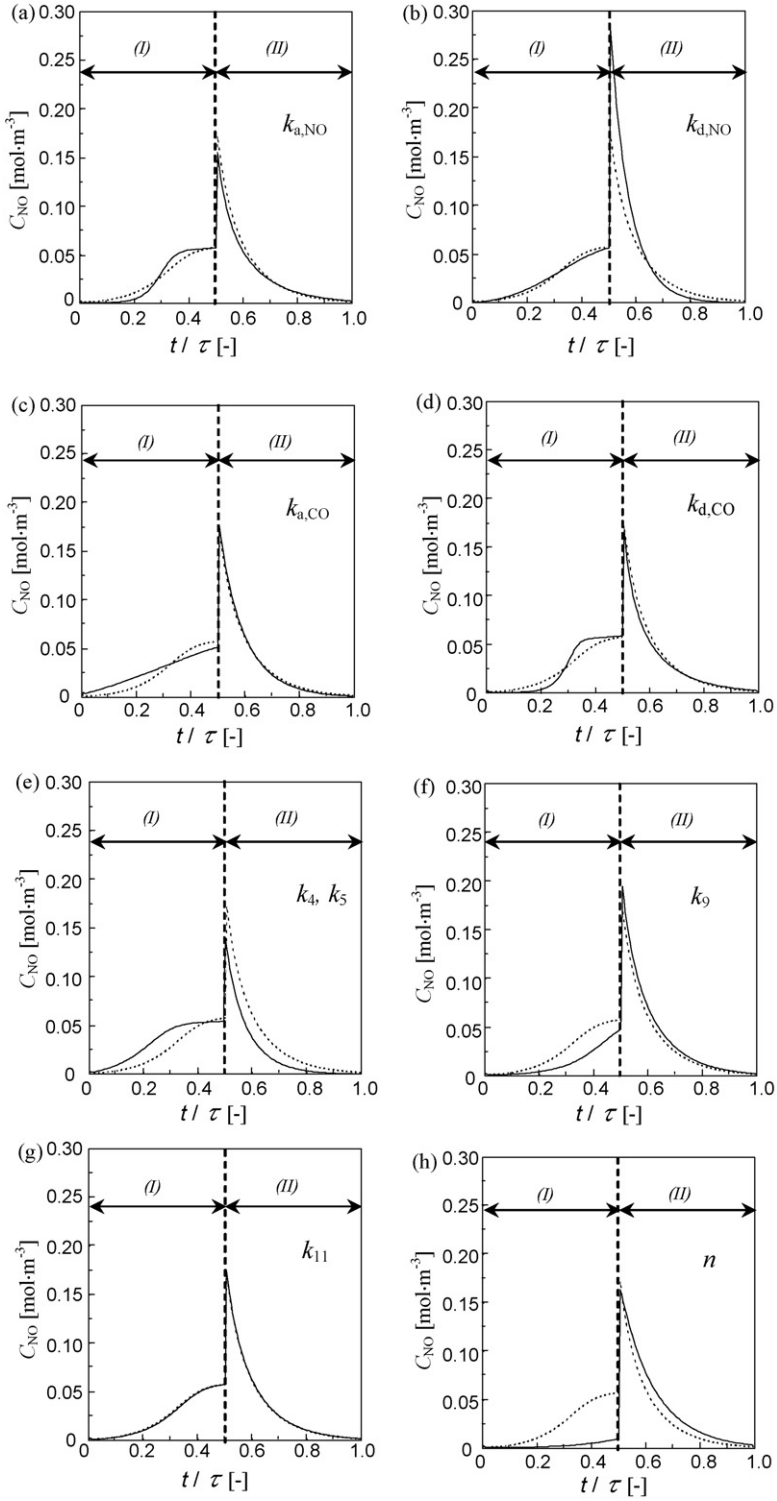

Fig. 10. Sensitivity of each parameter in Mechanism II to the shape of C_{NO} wave at the reactor outlet: the calculated result using (- - -) the parameter listed in Table 4; (—) the double value of the parameter listed in Table 4.

and K_{CO} are very large. This indicates that both NO and CO were strongly adsorbed onto the active sites. Moreover, $k_{d,CO}$ is about 7 times greater than $k_{d,NO}$. This indicates that the adsorbed CO desorbed more easily than the adsorbed NO. The parameter for each step in the reversible adsorptions of NO and CO gives good agreement with the comparative adsorption strengths of NO and CO on Rh sites [10,20,22,40,42]. The smallest rate constant of the surface reactions is k_{11}. This means that the recombination of N-s is the rate-determining step of the overall reduction of NO. This gives good agreement with the product distribution observed at the steady state and the works reported in the literature; the selectivity of N_2O is higher than that of N_2 when NO reacts with CO at the temperature below light-off temperature [15,20,47,3,63]. The number of active sites, n, obtained from the simulation corresponds to 21.1%

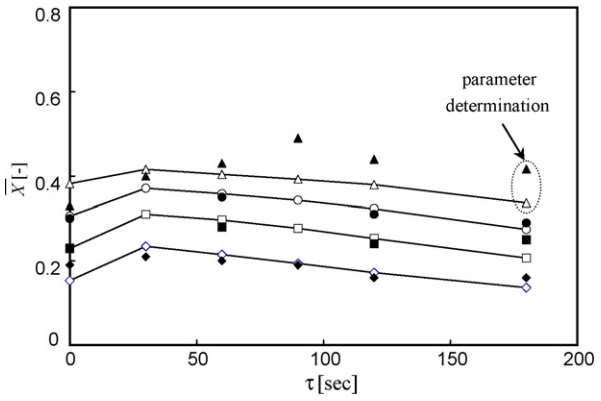

Fig. 11. Effect of cycling period on time-averaged conversion of NO for W: (♦, –◇–) 0.2 g; (■, –□–) 0.3 g; (●, ···○···) 0.4 g; (▲, - -△- -) 0.5 g. Symbols were given for the experimental results. Curves were for the calculated results.

of the total amount of Rh atoms loaded in 1 wt% of Rh/Al_2O_3. The low value of "n" should be explained by the accumulation of dicarbonyl on the Rh sites. As described in Section 3.2, the sites occupied by two molecules of CO ($Rh(CO)_2$) cannot participate the catalytic cycle.

In order to evaluate the model reliability, we conducted the periodic operation experiments for various weights of catalyst (W) and used the obtained parameters and Mechanism II to calculate $\bar{X}_{NO}$ for various conditions. Fig. 11 shows the experimental results comparing with the calculated ones. It should be noted that only the points in the dotted-cycle ($\tau = 180$ s, $W = 0.5$ g) were employed to determine the kinetic parameters in Section 3.3. The calculated curves simulated the effect of a cycling period on $\bar{X}_{NO}$ reasonably well especially when $\bar{X}_{NO} < 0.4$. The deviation from the assumption of isothermal condition should be a reason for the difference between the calculated results and the experimental ones when $\bar{X}_{NO}$ was larger than 0.4. In conclusion, the obtained mechanism and its parameter should be well enough to predict both steady and periodic behaviors of the reaction.

This work demonstrates the way to establish a practical kinetic model which is well enough to explain the performance of such a complicated reaction under both steady and unsteady conditions. Since the distribution of surface coverage under the unsteady condition may be completely different from that at the steady state, a steady-state kinetics model may be unable to predict unsteady performance. For such a case, our proposed method should be useful to get better understanding on the kinetics of the reaction. Until now, there have been several efforts performed in order to improve the performance of automotive catalytic converters especially under cold start conditions. The performance of bimetallic catalysts, other noble metal catalysts (e.g. Pd, Ir) and supported noble metal catalysts with oxygen carrier promoter have been investigated for NO–CO, NO–CO–O_2, N_2O–CO, CO–O_2 and NO–CO–HC reactions [6,64–68]. Since in these reaction systems strong adsorption of reactants has been widely reported in the literature especially under the low temperatures, the deformation of a concentration wave of reactants should be expected. Analyzing the shape of the deformed wave of reactant concentration should give meaningful information on kinetics of the reaction.

4. Conclusions

A reaction mechanism and kinetic parameters of NO–CO reaction over Rh/Al_2O_3 at 423 K were obtained from the simulations of both steady-state rate data and periodic performance. It was found that the reaction between NO and CO molecules occurred via Eley–Redial-like mechanism. N_2O is formed by the reaction between NO-s and N-s whereas N_2 is formed by the recombination of N-s. Production rate of N_2 is much slower than that of N_2O. The mechanism and the rate parameters obtained according to the proposed method can reproduce important characteristics of steady and periodic behaviors of the reaction reasonably well. In order to study kinetics of this reaction and determine an adequate set of rate parameters, analysis of both steady and bang–bang periodic behavior is necessity. The proposed method is effective for studying kinetics of such a complicated reaction.

Acknowledgement

The authors gratefully acknowledge the financial supports by Thailand Research Fund (TRF) through the grant number MRG4680085 and Faculty of Engineering, King Mongkut's Institute of Technology Ladkrabang.

References

[1] K.C. Taylor, Catal. Rev.-Sci. Eng. 35 (1993) 457.
[2] M. Shelef, G.W. Graham, Catal. Rev.-Sci. Eng. 36 (1994) 433.
[3] V.P. Zhdanov, B. Kasemo, Surf. Sci. Rep. 29 (1997) 31.
[4] V.I. Pârvulescu, P. Grange, B. Delmon, Catal. Today 46 (1998) 233.
[5] D.N. Belton, K.C. Taylor, Curr. Opin. Solid State Mater. Sci. 4 (1999) 97.
[6] P. Granger, C. Dujardin, J.-F. Paul, G. Leclercq, J. Mol. Catal. A-Chem. 228 (2005) 241.
[7] P.L. Silveston, Catal. Today 25 (1995) 175.
[8] K.C. Taylor, R.M. Sinkevitch, Ind. Eng. Chem. Prod. Res. Dev. 22 (1983) 45.
[9] H. Muraki, H. Shinjoh, H. Sobukawa, K. Yokota, Y. Fujitani, Ind. Eng. Chem. Prod. Res. Dev. 24 (1985) 43.
[10] H. Muraki, Y. Fujitani, Ind. Eng. Chem. Prod. Res. Dev. 25 (1986) 414.
[11] T. Aida, D. Na-Ranong, R. Kobayashi, H. Niiyama, Chem. Eng. Sci. 54 (1999) 4449.
[12] D. Mantri, P. Aghalayam, Catal. Today 119 (2007) 88.
[13] L.A. Avalos, V. Bustos, R. Uñac, F. Zaera, G. Zgrablich, J. Phys. Chem. 110 (2006) 24964.
[14] S.J. Alas, L. Vicente, J. Mol. Catal. A-Chem. 281 (2008) 24.
[15] R.R. Sadhankar, D.T. Lynch, Ind. Eng. Chem. Res. 36 (1997) 4609.
[16] R.R. Sadhankar, D.T. Lynch, Chem. Eng. Sci. 51 (1996) 2061.
[17] L.A. Avalos, V. Bustos, R. Uñac, F. Zaera, G. Zgrablich, J. Phys. Chem. B 110 (2006) 24964.
[18] K. Almusaiteer, S.S.C. Chuang, J. Catal. 184 (1999) 189.
[19] D. Na-Ranong, T. Aida, H. Niiyama, Appl. Catal. A-Gen. 234 (2002) 103.
[20] W.C. Hecker, A.T. Bell, J. Catal. 84 (1983) 200.
[21] H. Arai, H. Tominaga, J. Catal. 43 (1976) 131.
[22] K.A. Alumusaiteer, S.S.C. Chuang, C.-D. Tan, J. Catal. 189 (2000) 247.
[23] T. Bansagi, T.S. Zakar, F. Solymosi, Appl. Catal. B-Environ. 66 (2006) 147.
[24] E.A. Hyde, R. Rudham, J. Chem. Soc.-Faraday Trans. I 80 (1984) 531.
[25] D. Na-Ranong, T. Yoshiga, T. Aida, H. Niiyama, The Proceedings of Chem. and Proc. Eng. Conf. (CPEC) 2000 in Conjunction with Regional Symposium Chem. Eng. (RSCE), Singapore, 2000.
[26] A.C. Yang, C.W. Garland, J. Phys. Chem. 61 (1957) 1504.
[27] J.T. Yates Jr., T.M. Duncan, S.D. Worley, R.W. Vaughan, J. Chem. Phys. 70 (1979) 1219.
[28] C. Wong, R.W. McCabe, J. Catal. 107 (1987) 535.
[29] R. Dictor, J. Catal. 109 (1988) 89.
[30] Y.E. Li, R.D. Gonzalez, J. Phys. Chem. 92 (1988) 1589.
[31] D.K. Paul, J.T. Yates Jr., J. Phys. Chem. 95 (1991) 1699.
[32] L. Conners, T. Hollis, D.A. Johnson, G. Blyholder, J. Phys. Chem. B 102 (1998) 10112.
[33] W.F. Banholzer, R.I. Marsel, Surf. Sci. 137 (1984) 339.
[34] N.W. Cant, R.A. Donaldson, J. Catal. 78 (1982) 461.
[35] D.S. Dunn, W.G. Golden, M.W. Severson, J. Overend, J. Phys. Chem. 84 (1980) 336.
[36] J.-L. Freysz, J. Saussey, J.-C. Lavalley, P. Bourges, J. Catal. 197 (2001) 131.
[37] P. Granger, C. Dathy, J.J. Lecomte, L. Leclercq, M. Prigent, G. Mabilon, G. Leclercq, J. Catal. 173 (1998) 304.
[38] B.E. Hayden, Surf. Sci. 131 (1983) 419.
[39] D. Lorimer, A.T. Bell, J. Catal. 59 (1979) 223.
[40] D. Na-Ranong, Ph.D. Thesis, Tokyo Institute of Technology, 2002.
[41] R.E. Hendershot, R.S. Hansen, J. Catal. 98 (1986) 150.
[42] P. Granger, J.J. Lecomte, C. Dathy, L. Leclercq, G. Leclercq, J. Catal. 175 (1998) 194.
[43] S.H. Oh, J.E. Carpenter, J. Catal. 101 (1986) 114.
[46] R.E. Lakis, Y. Cai, H.G. Stenger, C.E. Lyman, J. Catal. 154 (1995) 276.
[47] D.N. Belton, S.J. Schmieg, J. Catal. 144 (1993) 9.
[48] G. Srinivas, S.S.C. Chaung, S. Debnath, J. Catal. 148 (1994) 748.
[49] J.A. Anderson, G.J. Millar, C.H. Rochester, J. Chem. Soc.-Faraday Trans. 86 (1990) 571.

[50] M.A. Newton, D.G. Burnaby, A.J. Dent, S.D. Moreno, J. Evans, S.G. Fiddy, T. Neisius, S. Turin, J. Phys. Chem. B 106 (2002) 4214.
[51] H. Arai, Ind. Eng. Chem. Prod. Res. Dev. 79 (1980) 507.
[52] L.H. Dubois, P.K. Hansma, G.A. Somorjai, J. Catal. 65 (1980) 318.
[53] L.A. Avalos, V. Bustos, R. Unac, F. Zaera, G. Zgrablich, J. Mol. Catal. A-Chem. 228 (2005) 89.
[54] H.J. Borg, J.F.C.-J.M. Reijerse, R.A.V. Santen, J.M. Niemantsverdriet, J. Chem. Phys. 101 (1994) 10052.
[55] D.N. Belton, C.L. DiMaggio, S.J. Schmieg, K.Y.S. Ng, J. Catal. 157 (1995) 559.
[56] K.Y.S. Ng, D.N. Belton, S.J. Schmieg, G.B. Fisher, J. Catal. 146 (1994) 394.
[57] D.K. Paul, S.D. Worley, N.W. Hoffmann, D.H. Ash, J. Gautney, Surf. Sci. 223 (1989) 509.
[58] D.I. Kondarides, T. Chafik, X.E. Verykios, J. Catal. 191 (2000) 147.
[59] D.I. Kondarides, T. Chafik, X.E. Verykios, J. Catal. 193 (2000) 303.
[60] F. Solymosi, T. Bansagi, J. Catal. 202 (2001) 205.
[61] D.I. Kondarides, X.E. Verykios, J. Catal. 202 (2001) 207.
[62] R. Krishnamurthy, S.S.C. Chuang, M.W. Balakos, J. Catal. 157 (1995) 512.
[63] V.P. Zhdanov, B. Kasemo, Surf. Sci. 496 (2002) 251.
[64] W. Ahmad, E.V. Albano, Appl. Surf. Sci. 254 (2008) 2436.
[65] P. Granger, P. Malfoy, G. Leclercq, J. Catal. 223 (2004) 142.
[66] P. Granger, J.J. Lecomte, L. Leclercq, G. Leclercq, Appl. Catal. A-Gen. 218 (2001) 257.
[67] P.-A. Carlsson, S. Mollner, K. Arnby, M. Skoglundh, Chem. Eng. Sci. 59 (2004) 4313.
[68] T. Fujitani, I. Nakamura, A. Takahashi, M. Haneda, H. Hamada, J. Catal. 253 (2008) 139.